Atmos. Meas. Tech. Discuss., 6, 10699–10730, 2013
www.atmos-meas-tech-discuss.net/6/10699/2013/
doi:10.5194/amtd-6-10699-2013
© Author(s) 2013. CC Attribution 3.0 License.

Atmospheric Measurement Techniques Discussions

Open Access

This discussion paper is/has been under review for the journal Atmospheric Measurement Techniques (AMT). Please refer to the corresponding final paper in AMT if available.

The large-scale spatio-temporal variability of precipitation over Sweden observed from the weather radar network

A. Devasthale and L. Norin

Atmospheric Remote Sensing Unit, Research and Development Department,
Swedish Meteorological and Hydrological Institute (SMHI), Norrköping, Sweden

Received: 24 November 2013 – Accepted: 2 December 2013 – Published: 11 December 2013

Correspondence to: A. Devasthale (abhay.devasthale@smhi.se)

Published by Copernicus Publications on behalf of the European Geosciences Union.

CC BY

Abstract

Using measurements from the national network of 12 weather radar stations for the last decade (2000–2010), we investigate the large-scale spatio-temporal variability of precipitation over Sweden. These statistics provide useful information to evaluate regional climate models as well as for hydrology and energy applications. A strict quality control is applied to filter out noise and artifacts from the radar data. We focus on investigating four distinct aspects namely, the diurnal cycle of precipitation and its seasonality, the dominant time scale (diurnal vs. seasonal) of variability, precipitation response to different wind directions, and the correlation of precipitation events with the North Atlantic Oscillation (NAO) and the Arctic Oscillation (AO). When classified based on their intensity, moderate to high intensity events (precipitation $> 0.34\,\mathrm{mm\,(3\,h)^{-1}}$) peak distinctly during late afternoon over the majority of radar stations in summer and during late night or early morning in winter. Precipitation variability is highest over the southwestern parts of Sweden. It is shown that the high intensity events (precipitation $> 1.7\,\mathrm{mm\,(3\,h)^{-1}}$) are positively correlated with NAO and AO (esp. over northern Sweden), while the low intensity events are negatively correlated (esp. over southeastern parts). It is further observed that southeasterly winds often lead to intense precipitation events over central and northern Sweden, while southwesterly winds contribute most to the total accumulated precipitation for all radar stations. Apart from its operational applications, the present study demonstrates the potential of the weather radar data set for studying climatic features of precipitation over Sweden.

1 Introduction

Precipitation is one of the important components in the global- and regional water- and energy cycles and one that has profound influence on human lives from daily to seasonal time scales. From a climate perspective, the changes in precipitation characteristics such as distribution, frequency, and amount and variability therein can have

CC BY

significant consequences for the long-term planning and consumption of the resources. Therefore, considering the importance of precipitation properties, global and regional climate models often strive to capture their statistical nature as accurately as possible so as to better predict any future changes (Dai, 2006).

From an observational perspective, tools such as rain-gauges (Schneider et al., 2012), weather radars (Huuskonen et al., 2013; Zhang et al., 2013), and satellite sensors (Adler et al., 2003) can be employed to monitor and document precipitation behaviour. In recent years, considerable efforts have been dedicated to produce climate quality observational data records of precipitation based solely on one of these tools or a combination of them. For a high latitude country like Sweden, weather radars offer a viable alternative to satellite observations and rain-gauge measurements. Satellite-based observations still suffer from limited accuracy over land (esp. at higher latitudes) and rain-gauge stations are spatially sparse. The high spatial and temporal resolutions of weather radars with their wide area coverage at near real time make them immensely useful for operational monitoring. The success stories of such applications can be seen from international initiatives such as and BALTRAD (http://www.baltrad.eu/).

In Sweden, apart from their operational use, more than a decade of continuous precipitation observations from weather radars located at 12 carefully chosen locations allow investigations of large-scale statistics of precipitation to gain insights into the climatic aspects. In the present study, this potential of the weather radar network is exploited to learn different aspects of precipitation variability. The focus is especially placed on presenting statistics that can be used for evaluating climate models. The next section describes the weather radar data set, its processing and quality control. Section 3 discusses the results and the final section presents the conclusions.

2 The weather radar data set

As a part of the Baltic Sea Experiment (BALTEX) the BALTEX Radar Data Center (BRDC) was established at the Swedish Meteorological and Hydrological Institute in

Discussion Paper | Discussion Paper | Discussion Paper | Discussion Paper |

1999. Since then, the BRDC collects and archives data from around 30 weather radars from countries adjacent to the Baltic Sea. The BRDC also generates radar-based products including radar reflectivity images of individual radars, composite images of radar reflectivity, and images for three and twelve hour accumulated precipitation (for details, see Michelson et al., 2000). In this study we have used the BRDC three hour accumulated precipitation images to investigate the diurnal and seasonal dependence of precipitation. As our main interest is precipitation over Sweden we have limited the images to areas covered only by the Swedish radars. However, as explained below, measurements very close to and very far from weather radars may have lower quality. We have therefore further limited the data to areas with radius $5\,\mathrm{km} < r < 80\,\mathrm{km}$ around the Swedish radars to improve the data quality.

The Swedish weather radar network consists of 12 horizontally polarized Ericsson C-band Doppler radars, providing almost complete national coverage (see Fig. 1 and Table 1). The radars measure reflectivity, radial velocity, and spectrum width. The radar reflectivity, Z, is measured by the radars in units of dBZ. The Swedish weather radars have a dynamic range of 8 bits and measures Z between -30 dBZ and 71.6 dBZ. To protect the radar receiver from overload the signal is damped by 60 dB near the radar, making the data of the first two range bins unusable. The radars have a half-power beam width of 0.9° and two pulse repetition frequencies are used to increase the maximum unambiguous velocity for the wind field measurements. The data processing managed by the radar signal processor and the data are output in matrices consisting of 120×420 radar cells for every elevation scan. The radial resolution of each radar cell is 2 km for the lowest four elevation angles and 1 km for the others. The azimuthal resolution of a cell is $360/420 \approx 0.86°$ for all elevation angles. The radars perform azimuthal scans of 360° around a vertical axis for 10 elevation angles, from 0.5° to 40°. Together, these scans make up polar volume data sets which are provided with an update time of 15 min. More technical characteristics of the radars are summarized in Table 2.

From the polar volume data sets horizontal cross sections of radar reflectivity at a certain altitude can be generated. Such cross sections are referred to as constant

AMTD
6, 10699–10730, 2013

CC BY

altitude plan polar indicator (CAPPI). A similar product is the pseudo-constant altitude plan polar indicator (PCAPPI) which is defined as the CAPPI where available, and over areas where no data exist at the specified altitude the measurement nearest in height is selected. At the BRDC the PCAPPI is defined at 500 m altitude above the corresponding radar.

The BRDC three hour accumulated precipitation composite image is generated by converting the radar reflectivity factor to rain rate for individual PCAPPI images, summing the images, adjusting the rain rate using rain gauge measurements, and finally compositing the images. The composite image has a spatial resolution of 2 km × 2 km. At the BRDC the radar reflectivity factor is converted to rain rate R (mm h^{-1}) using the empirical relationship $Z = aR^b$ (see, e.g. Battan, 1973), with $a = 400, b = 2$ for the cold season (October to March) and $a = 200, b = 1.5$ for the warm season (April to September).

Measurements at increasing distances from the radars are made at increasing heights (with increasing risk of overshooting precipitating clouds). Measurements made at large distances from the radar may therefore be of lower quality. Rain gauge measurements, which are considered to produce high quality point measurements, are therefore used to calibrate the summed radar images and to adjust for any distance dependence. Rain gauge observations are available at 06:00 and 18:00 UTC every day.

The gauge adjustment method relies on the logarithmic gauge-to-radar ratio. The BRDC use all such point pairs available within the last seven days to fit a second degree polynomial with respect to distance from the nearest radar. The seven days window is used to ensure that enough data points exist. Only radar measurements above 0.1 mm and rain gauge measurements above 0.5 mm are taken into account. For details on the gauge adjustment method, see Michelson and Koistinen (2000).

In order to remove radar echoes not originating from precipitation the BRDC applies a filer using satellite observations is applied. In areas classified as cloud free

AMTD
6, 10699–10730, 2013

by the satellite observations this filter removes all radar echoes. For details, see Michelson (2006).

Obstacles such as high buildings or mountains in line-of-sight of radar may yield large reflections (clutter) that the built-in clutter filters are sometimes unable to suppress completely. This can occasionally leave unreasonably large precipitation values in the data. For the purpose of this study we have therefore, in addition to the above described quality controls employed by the BRDC, applied a filter that removes any radar cell that on a given month or year shows an accumulated precipitation higher than 500 mm month^{-1} or 2000 mm yr^{-1} (the highest amounts ever recorded by rain gauges in Sweden are 429 mm month^{-1} and 1866 mm yr^{-1}).

In this study we have used all pixels from the composite images found within a radius of 5–80 km around each of the 12 Swedish radar stations to generate data sets of accumulated precipitation every 3 h. The number of pixels for any radar station is approximately 5150. However, the above described filter can reduce the actual number of pixels on a given year and month. Figure A1 shows the number of pixels used for each of the radars as a function of time. For the majority of the time, the numbers of pixels removed were far fewer and the average number of pixels used per month per radar was 5024. The smallest number of pixels for any radar at any time was 3499, which is still more than enough to statistically represent rainfall distribution (the calculated margin of error remains less than 1.6 %). Furthermore, probability distribution functions (PDF) of rainfall for all stations look very similar (as reflected in Fig. 3), in spite of different number of samples. We have also inspected the PDF for radar stations during periods of less data and compared to the corresponding PDF for periods with near full coverage. The difference between these PDFs is negligible. These aspects give us confidence that the sampling errors are least likely to influence our results.

Since the main goal of the present study is to learn more about the large-scale features, the spatial information of the pixels around an individual radar station is not used in the analysis.

AMTD
6, 10699–10730, 2013

CC BY

3 The spatio-temporal variability of precipitation

We focus on investigating four distinct aspects of the spatio-temporal variability in precipitation in the present study. First, we examine the diurnal cycle of precipitation and its seasonality. Then, we investigate the dominant time scale (diurnal vs. seasonal) of the precipitation variability. Further the correlation of precipitation with the major modes of natural variability in the Northern Hemisphere, i.e. the North Atlantic Oscillation (NAO) and the Arctic Oscillation (AO) is examined. And finally, we investigate the influence of wind direction on the observed precipitation amount.

3.1 Diurnal variations in precipitation

Simulating the diurnal cycle of precipitation accurately is one of the main challenges faced by climate models. For example, coupled climate models have a tendency to produce convective precipitation too early and too frequent compared to observations during warm season (Dai, 2006; Jeong et al., 2011). In general, the diurnal cycle of precipitation depends on many factors, such as geographical position, season, surface characteristics etc. But perhaps the most governing and dynamical factor influencing diurnal cycle is the role of atmospheric conditions leading to precipitation. For example, spatio-temporal characteristics of precipitation are quite different during the passage of frontal systems as opposed to those during local convection. This is especially true for Sweden where both the frontal systems and local convection contribute to the total annual precipitation.

In their study Walther and Bennartz (2006) showed that, over the Baltic Sea region (where Sweden shares a very long coastline), precipitation events attributed to the frontal systems constitute two-thirds of all events. However, they also observed strong seasonal variability in the number of precursor frontal systems. For example, the fraction of non-frontal systems was by a factor of 2–3 higher during the summer half of the year. This aspect certainly influences the diurnal cycle of precipitation. For example, the peak time of diurnal cycle will vary considerably from one synoptic event to

AMTD
6, 10699–10730, 2013

another depending on the dynamical state of the atmosphere and surface interactions during the passage of the frontal system over the study region. However, during peak summer, strong surface heating and moisture availability leads to well-defined diurnal cycle of convection (and the resulting precipitation) that usually peaks during the late afternoon or early evening. This intrinsic variability in the peaks of diurnal cycle is evident in Fig. 2, which shows the diurnal cycle of precipitation for the 12 radar stations over Sweden during four seasons. It also provides an overview of absolute precipitation frequency and its seasonality for different stations. Only in the summer season the majority of stations show diurnal cycles peaking at same time (15–18 h), while in the winter season, there is no clear diurnal peak time tendency across the stations. The other two seasons show mixed peak times. The majority of stations show well-defined and higher amplitudes in precipitation frequency during summer, while the diurnal cycles are quite flatter in other seasons, especially in spring.

Often times it is of more interest to understand when the precipitation events with different intensities peak during different seasons. This information is not only useful to evaluate climate models, but also for hydrology and for the planning of resources and energy. Therefore, as shown in Fig. 3, we classified three hour precipitation accumulations into 8 categories based on their intensities. The bin size is chosen in such a way that there are roughly the same numbers of samples in each bin, thus making statistical comparison more robust. Table 3 summarizes the boundaries of each intensity bin. Such classification of precipitation events provides us more detailed knowledge of the timing of their occurrence at different intensities. Figure 4 shows the results of this analysis. In winter and spring, there is no clear general tendency in the timing of precipitation peak across radar stations and intensity bins. It is to be kept in mind that, as shown in Fig. 2, the diurnal cycles of total precipitation during these months are quite flat. The processes leading to precipitation do not depend, to a first order, on the local scale diurnal variations and thus do not result into any preferred timing of peak in rainfall. In summer, the majority of stations show late afternoon peak for low and moderate intensity events. In autumn the low intensity events peak during late night or

AMTD
6, 10699–10730, 2013

CC BY

early morning. In the majority of the cases, the highest intensity events (bin 8) occur between late evenings to early morning irrespective of the season.

Our results for the diurnal cycle of total precipitation are in general agreement with the comprehensive study by Jeong et al. (2011), who use data from the network of rain gauge stations across Sweden. Our value addition lies in the fact that we further classify precipitation based on intensity to investigate diurnal cycles and also that we analyse the four seasons separately. Furthermore, our analysis is based on a completely different observational platform.

3.2 Diurnal vs. seasonal variability

Since precipitation is a result of various thermodynamical and radiative processes and their couplings and interactions with each other, a great deal of confidence can be placed in a climate model if it is able to simulate precipitation variability at various spatio-temporal scales. The coefficient of variation (COV, defined as standard deviation divided by mean) is a simple yet very powerful statistical metric to study precipitation variability. It facilitates comparison for the quantities that could have different sample means, as in the case of the present study, where there is large precipitation variability across radar stations (e.g. refer Fig. 2). In Fig. 5, COV is expressed as a function of each 3 h time bin and season for each of the 12 radar stations. This not only provides us an overview of precipitation variability across all stations, but more importantly, allows us to compare whether the diurnal or seasonal variability is more important for an individual station.

The highest precipitation variability is observed over southwestern Sweden, central eastern Sweden and the northernmost parts of the country. On the other hand, lower precipitation variability is observed over the southeastern parts. The northeastern parts of the country also experience lower variability. There is also a general tendency that the seasonal variations in precipitation are stronger during late nights and early mornings (time bins 1 and 8).

AMTD
6, 10699–10730, 2013

cc BY

3.3 Correlation with NAO and AO indices

The North Atlantic Oscillation (NAO) and the Arctic Oscillation (AO) are considered to be dominant modes of atmospheric variability in the Northern Hemisphere (Hurrell, 1995; Thompson and Wallace, 1998; Christianson, 2002). The NAO and AO indices are defined by taking into consideration different physical metrics. While the emphasis is placed on the strength of atmospheric circulation over the Arctic and the resulting geopotential height anomalies in defining the AO index, the state of the two pressure systems in the North Atlantic Ocean (one over the Icelandic region and the other over Azores) is taken into account while defining the NAO index. There exists debate as to which one of these oscillatory systems can be understood in a physically meaningful way (Ambaum et al., 2001). However, there is no ambiguity with regard to their influence on the climates of the North Atlantic Ocean and surrounding continents. They have first order impact on the observed inter-annual changes in the water and energy cycle over these regions. This also applies to the Scandinavian region, especially during the winter half of a year.

The changes in the meridional temperature gradient and strengthening/weakening of westerlies during different phases of these oscillations eventually determine the advection of heat and moisture across the North Atlantic and the neighbouring continents. In general it is observed that during their positive phases, the winter storms are more frequent and extend over northern Europe, especially Scandinavia. Chen (2001), Linderson (2001) and Hellström (2005) have analysed different weather states and circulation patterns over Sweden. Chen (2001) and Linderson (2001) have shown that, during winter (when NAO/AO are most active), westerly and southwesterly winds are often dominating the weather state classification.

Figure 6 provides an overview of meteorological conditions during strongly positive ($> 1\sigma$) and negative phases ($< -1\sigma$) of the Arctic Oscillation over northern Europe. It shows the dominant wind patterns and temperature and water vapour anomalies at 850 hPa for 2002–2012. The wind data are obtained from the ECMWF's ERA-Interim

CC BY

reanalysis (Dee et al., 2011), while temperature and water vapour retrievals from the Atmospheric Infrared Sounder (AIRS) sensor onboard NASA's Aqua satellite are used for analysis (Chahine et al., 2006; Fetzer, 2006). It can be clearly seen that, during positive phases, strong westerly/southwesterly winds bring heat and moisture towards Scandinavian region as evident in the positive temperature and water-vapour anomalies, while the opposite is true during negative phases. As the contribution of convective precipitation to the total is very small over Sweden during winter due to the lack of solar heating, the frontal systems remain the dominant driver behind the observed anomalies in temperature and water vapour and thus the source of precipitation (e.g. Walther and Bennartz, 2006). Since these systems are in turn heavily influenced by NAO and AO indices, the precipitation response to both indices is also expected. This aspect is investigated in the present study and the results are shown in Fig. 7. We divided precipitation events into three categories based on their intensity, namely low (intensity $\leq 0.34\,\mathrm{mm}\,(3\,\mathrm{h})^{-1}$), medium ($0.34 <$ intensity $\leq 1.7\,\mathrm{mm}\,(3\,\mathrm{h})^{-1}$) and high $> 1.7\,\mathrm{mm}\,(3\,\mathrm{h})^{-1}$), with the further aim of understanding whether different intensity events respond differently to the changes in large-scale circulation represented by the NAO and AO indices. Figure 7 shows the correlation of accumulated monthly precipitation with these indices (left column) for two scenarios, first when only the DJF months are included in the analysis (top two rows) and the other when the NDJFM months are included (bottom two rows). The subplots in the right column show confidence levels at which these correlations are significant. It is indeed interesting to note that for the majority of the radar stations, high intensity precipitation events are positively correlated with the monthly NAO and AO indices. The low intensity events, on the other hand, are negatively correlated. The statistical significance of these correlations is also very high. In particular, high intensity events over northern Sweden are strongly positively correlated with AO/NAO indices, while low intensity events over southeastern Sweden are strongly negatively correlated. When November and March months are included in the analysis, the general tendency of positive/negative correlation with high/low intensity events becomes even stronger. The results point out the influence of AO/NAO on the

AMTD
6, 10699–10730, 2013

CC BY

precipitation patterns over Sweden. Considering the fact that nearly 50 % of energy production in Sweden is based on hydropower, where precipitation plays an important role, any future change in the influence of AO/NAO on precipitation will likely have an impact on the national energy policy (Cherry et al., 2005). Further regional modeling studies are required to investigate these aspects in detail.

A few previous studies have investigated the influence of large-scale circulation on Swedish precipitation (e.g. Busuioc et al., 2001; Johansson and Chen, 2003; Uvo, 2003; Hellström, 2005; Gustafsson et al., 2010). Particularly, Busuioc et al. (2001) and Uvo (2003) analysed the relationship of NAO with precipitation over Sweden. It is difficult to directly compare our results with these studies due to different study periods, lengths of data records, and regimes of NAO. Nevertheless, it is interesting to note some similarities, for example, relatively high correlations over northern Sweden and low correlations over southeastern Sweden. By partitioning the precipitation events into low, medium and high categories and by analyzing the precipitation record for the most recent decade, here, we complement these earlier studies.

3.4 Rainfall response to wind direction

Having detailed knowledge of rainfall response to wind direction is important for a country like Sweden where varied directional interplay of meteorology, topography and neighbouring oceanic regimes eventually determines the longevity of frontal systems and the amount of moisture transport in the atmosphere. For example, the conditions are often conducive for precipitation when strong and moist winds from westerly direction (North Atlantic/North Sea origins) arrive over land, compared to conditions under dryer and colder winds of northeasterly origin. Figures 8 and 9 show the probability density function of wind direction and the corresponding mean wind strength over the locations of the 12 radar stations. It is evident that in general westerly winds dominate over all locations irrespective of season. In northern Sweden, both northwesterly and southwesterly winds dominate, and in southern Sweden, westerly and southwesterly winds are most frequent. In comparison to wind direction, the distribution of wind

AMTD
6, 10699–10730, 2013

CC BY

strength is much uniform across all stations. During autumn and winter, winds are generally stronger.

In order to investigate response of precipitation to these prominent wind directions, we pose ourselves two questions;

a. For a given radar location, which wind direction is likely to produce high average daily rain rate?

b. For a given radar location, which wind direction leads to most frequent precipitation occurrence?

To answer the first question, Fig. 10 shows the relative contribution of four wind directions to average seasonal rainfall intensity, while Fig. 11 shows the same after normalizing by total number of precipitation events to address the second question.

Figure 10 shows a clear tendency that in northern Sweden (station 1 up to station 7) southeasterly winds are mainly responsible for the highest daily rain rate (nearly 40 % of the time), while in the southern Sweden it is southwesterly winds that lead to the highest daily rain rate events. The latter is especially true for stations near the southwestern coast. In case of the northerly stations, Norwegian mountain ranges along Sweden's western border hinder frontal systems from producing high daily rainfall (in seasonal average). But when southeasterly winds coming from the continental Europe pick up moisture over the Baltic Sea, they have higher potential for producing high daily rain rate events. In summer, even the southern stations are influenced by south- or northeasterly winds. Station 9, located on the island Gotland in the Baltic Sea, shows an interesting seasonality. In summer, southeasterly winds are responsible for producing nearly half of all highest daily rain rate events, while in autumn, the contribution from northeasterly winds is slightly higher. In winter, the contribution from southerly and easterly winds is nearly equal.

Although winds originating from southeasterly direction often lead to intense precipitation events, Fig. 11 interestingly shows that southwesterly winds contribute most to the total accumulated rainfall. This in general holds true for all stations during all

AMTD
6, 10699–10730, 2013

CC BY

seasons, although this tendency is more clearly observed over southern Sweden compared to northernmost parts of the country.

4 Conclusions and outlook

With their accurate measurements of precipitation and high spatio-temporal resolution, weather radars are being routinely used for operational meteorological applications since many years. As a part of the BALTRAD project, the network connecting 12 such radars is operational in Sweden since more than a decade covering almost the entire country. Besides its operational use, the valuable decade long data record from these radars is underutilized for other applications.

In the present study we exploit this decade long (2000–2010) data record to study climatic features of precipitation over Sweden. Four aspects relevant for climate applications and evaluation of regional climate models are investigated, namely diurnal cycle, seasonal vs. diurnal variability, influence of NAO and AO on precipitation, and finally precipitation response to wind direction. It is observed that the majority of the radar stations show diurnal cycles peaking during later afternoon in summer, while there is no such general tendency during other seasons. When the precipitation events are categorized based on intensity, there is a general tendency that the moderate and high intensity events also occur during late afternoon in summer, while they peak during late night or early morning in winter. The high intensity events (precipitation $> 1.7\,\mathrm{mm}\,(3\,\mathrm{h})^{-1}$) over the majority of the radar stations are positively correlated with the NAO and AO indices, while the low intensity events are negatively correlated. The stations located in the northern parts of the country show high positive correlation, while the ones located in the southeastern parts show high negative correlation. This demonstrates the influence of large-scale advection on the total precipitation during different phases of the NAO and AO. It is further shown that southeasterly winds often lead to highest daily rain rate events over central and northern Sweden, while

CC BY

southwesterly winds contribute most to the total accumulated precipitation for all radar stations.

The present study demonstrates the potential of the weather radar network data set for climate applications over Sweden. Especially, these results are useful to evaluate the fidelity of regional climate models. Since radar based monitoring will continue for a long time in the future and since we can capitalize on the lessons learned from the experience of generating satellite based long-term cloud climatologies, this long-term data set could further provide deeper insights into other climatological features and trends in precipitation over Sweden in the future. In view of this, we plan to carry out a feasibility study to harmonize cross-calibration of radars in future, quantify uncertainties in precipitation estimates and facilitate the generation of climate quality data record from this radar network. We further plan to take a 3-tier approach where we aim to intercompare and harmonize rain gauge, radar, and satellite estimates of precipitation so as exploit the strengths of each observing system over Sweden.

Acknowledgements. The authors would like to thank those many who were/are involved in the establishment and running of the weather radar network over Sweden. ERA-Interim data was obtained from the ECMWF data center and AIRS-Aqua data obtained from the NASA ASDC. Abhay Devasthale acknowledges the support of Swedish National Space Board.

References

Adler, R. F., Huffman, G. J., Chang, A., Ferraro, R., Xie, P., Janowiak, J., Rudolf, B., Schneider, U., Curtis, S., Bolvin, D., Gruber, A., Susskind, J., and Arkin, P.: The version 2 Global Precipitation Climatology Project (GPCP) monthly precipitation analysis (1979–present), J. Hydrometeorol., 4, 1147–1167, 2003.

Ambaum, M. H. P., Hoskins, B. J., and Stephenson, D. B.: Arctic oscillation or North Atlantic oscillation?, J. Climate, 14, 3495–3507, 2001.

Battan, L. J.: Radar Observation of the Atmosphere, University of Chicago Press, 324 pp., 1973.

AMTD

6, 10699–10730, 2013

Precipitation variability over Sweden

A. Devasthale and L. Norin

Title Page
Abstract | Introduction
Conclusions | References
Tables | Figures
◂ | ▸
Back | Close
Full Screen / Esc
Printer-friendly Version
Interactive Discussion

Busuioc, A., Chen, D., and Hellström, C.: Temporal and spatial variability of precipitation in Sweden and its link with the large scale atmospheric circulation, Tellus A, 53, 348–367, 2001.

Chahine, M. T., Pagano, T. S., Aumann, H. H., Atlas, R., Barnet, C., Blaisdell, J., Chen, L., Divakarla, M., Fetzer, E. J., Goldberg, M., Gautier, C., Granger, S., Hannon, S., Irion, F. W., Kakar, R., Kalnay, E., Lambrigtsen, B. H., Lee, S.-Y., Le Marshall, J., McMillan, W. W., McMillin, L., Olsen, E. T., Revercomb, H., Rosenkranz, P., Smith, W. L., Staelin, D., Strow, L. L., Susskind, J., Tobin, D., Wolf, W., and Zhou, L.: AIRS: Improving Weather Forecasting and Providing New Data on Greenhouse Gases, B. Am. Meteorol. Soc., 87, 911–926, 2006.

Chen, D.: A monthly circulation climatology for Sweden and its application to a winter temperature case study, Int. J. Climatol., 20, 1067–1076, 2000.

Cherry, J., Cullen, H., Visbeck, M., Small, A., and Uvo, C.: Impacts of the North Atlantic Oscillation on Scandinavian hydropower Production and energy markets, Water Resour. Manag., 19, 673–691, doi:10.1007/s11269-005-3279-z, 2005.

Christiansen, B.: On the physical nature of the Arctic Oscillation, Geophys. Res. Lett., 29, 1805, doi:10.1029/2002GL015208, 2002.

Dai, A.: Precipitation characteristics in eighteen coupled climate models, J. Climate, 19, 4605–4630, 2006.

Dee, D. P., Uppala, S. M., Simmons, A. J., Berrisford, P., Poli, P., Kobayashi, S., Andrae, U., Balmaseda, M. A., Balsamo, G., Bauer, P., Bechtold, P., Beljaars, A. C. M., van de Berg, L., Bidlot, J., Bormann, N., Delsol, C., Dragani, R., Fuentes, M., Geer, A. J., Haimberger, L., Healy, S. B., Hersbach, H., Hólm, E. V., Isaksen, L., Kållberg, P., Köhler, M., Matricardi, M., McNally, A. P., Monge-Sanz, B. M., Morcrette, J.-J., Park, B.-K., Peubey, C., de Rosnay, P., Tavolato, C., Thépaut, J.-N., and Vitart, F.: The ERA-Interim reanalysis: Configuration and performance of the data assimilation system, Q. J. Roy. Meteorol. Soc., 137, 553–597, doi:10.1002/qj.828, 2011.

Fetzer, E. J.: Preface to special section: validation of atmospheric infrared sounder observations, J. Geophys. Res., 111, D09S01, doi:10.1029/2005JD007020, 2006.

Gustafsson, M., Rayner, D., and Chen, D.: Extreme rainfall events in southern Sweden: where does the moisture come from?, Tellus A, 62, 605–616, doi:10.1111/j.1600-0870.2010.00456.x., 2010.

Hellström, C.: Atmospheric conditions during extreme and non-extreme precipitation events in Sweden, Int. J. Climatol., 25, 631–648, 2005.

CC BY

Hurrell, J. W.: Decadal trends in the North Atlantic Oscillation: regional temperatures and precipitation, Science, 269, 676–679, 1995.
Huuskonen, A., Saltikoff, E., and Holleman, I.: The Operational Weather Radar Network in Europe, B. Am. Meteorol. Soc., online first, doi:10.1175/BAMS-D-12-00216.1, 2013.
Jeong, J.-H., Walther, A., Nikulin, G., Chen, D., and Jones, C.: Diurnal cycle of precipitation amount and frequency in Sweden: observation vs. model simulation, Tellus A, 63, 664–674, doi:10.1111/j.1600-0870.2011.00517.x, 2011.
Koistinen, J. and Michelson, D. B.: BALTEX weather radar-based products and their accuracies, Boreal Environ. Res., 7, 153–163, 2002.
Koistinen, J. and Puhakka, T.: An improved spatial gauge-radar adjustment technique, in: Preprints 20th AMS Conf. on Radar Met. 30 November–3 December 2001, Boston, MA, USA, 179–186, 1981.
Linderson, M.-J.: Objective classification of atmospheric circulation over southern Scandinavia, Int. J. Climatol., 21, 155–169, 2001.
Michelson, D.: The Swedish Weather Radar Production Chain, Proc. ERAD 2006, 2006.
Michelson, D. B. and Koistinen, J.: Gauge-radar network adjustment for the Baltic Sea Experiment, Phys. Chem. Earth, 25, 915–920, 2002.
Michelson, D. B., Andersson, T., Koistinen, J., Collier, C. G., Riedl, J., Szturc, J., Gjertsen, U., Nielsen, A., and Overgaard, S.: BALTEX Radar Data Centre Products and their Methodologies, SMHI Reports Meteorology and Climatology RMK Nr. 90. SMHI, SE-601 76, Norrköping, Sweden, 76 pp., 2000.
Schneider, U., Becker, A., Meyer-Christoffer, A., Ziese, M., and Rudolf, B.: Global Precipitation Analysis Products of the GPCC, Global Precipitation Climatology Centre (GPCC), DWD, Internet Publikation, 1–13, 2011.
Thompson, D. W. J. and Wallace, J. M.: The Arctic Oscillation signature in the wintertime geopotential height and temperature fields, Geophys. Res. Lett., 25, 1297–1300, 1998.
Zhang, J., Howard, K., Langston, C., Vasiloff, S., Kaney, B., Arthur, A., Van Cooten, S., Kelleher, K., Kitzmiller, D., Ding, F., Seo, D.-J., Wells, E., and Dempsey, C.: National Mosaic and Multi-Sensor QPE (NMQ) system: description, results, and future plans, B. Am. Meteorol. Soc., 92, 1321–1338, doi:10.1175/2011BAMS-D-11-00047.1, 2011.

CC BY

Table 1. Listing of weather radar stations over Sweden.

Station number	Station name	WMO ID	Latitude (°)	Longitude (°)	Altitude (m a.s.l.)
1	Kiruna	2032	67.7088	20.6178	647
2	Luleå	2092	65.4309	21.8650	68
3	Örnsköldsvik	2262	63.6395	18.4019	522
4	Östersund	2200	63.2951	14.7591	466
5	Hudiksvall	2334	61.5771	16.7144	389
6	Leksand	2430	60.7230	14.8776	457
7	Arlanda	2451	59.6544	17.9463	74
8	Vara	2600	58.2556	12.8260	164
9	Vilebo	2570	58.1059	15.9363	223
10	Ase	2588	57.3035	18.4001	85
11	Ängelholm	2606	56.3675	12.8517	209
12	Karlskrona	2666	56.2955	15.6103	123

AMTD

6, 10699–10730, 2013

Precipitation variability over Sweden

A. Devasthale and L. Norin

Table 2. Technical characteristics of the Swedish weather radars.

Elevation angles	0.5°, 1.0°, 1.5°, 2.0°	2.5°, 4.0°, 8.0°, 14°, 24°, 40°
Transmitted power	250 kW	250 kW
Wavelength	5.35 cm	5.35 cm
Gain	44.7 dB	44.7 dB
Pulse width	0.5 µs	0.5 µs
Beam width	0.9°	0.9°
PRFs	600/450 Hz	1200/900 Hz
Rotational speed	2 rpm	2 rpm
Measurement radius	240 km	120 km
Radial resolution	2 km	1 km
Azimuthal resolution	0.86°	0.86°
Range bins	120	120
Azimuth gates	420	420

Discussion Paper | Discussion Paper | Discussion Paper | Discussion Paper |

AMTD

6, 10699–10730, 2013

Precipitation variability over Sweden

A. Devasthale and L. Norin

Title Page
Abstract Introduction
Conclusions References
Tables Figures
◂ ▸
Back Close
Full Screen / Esc
Printer-friendly Version
Interactive Discussion

CC BY

AMTD
6, 10699–10730, 2013

Precipitation variability over Sweden

A. Devasthale and L. Norin

Table 3. Binning of precipitation intensity into 8 bins.

Bin	Precipitation intensity ($mm\,(3\,h)^{-1}$)
1	< 0.14
2	0.14–0.21
3	0.21–0.34
4	0.34–0.55
5	0.55–0.96
6	0.96–1.7
7	1.7–3.25
8	3.25–100

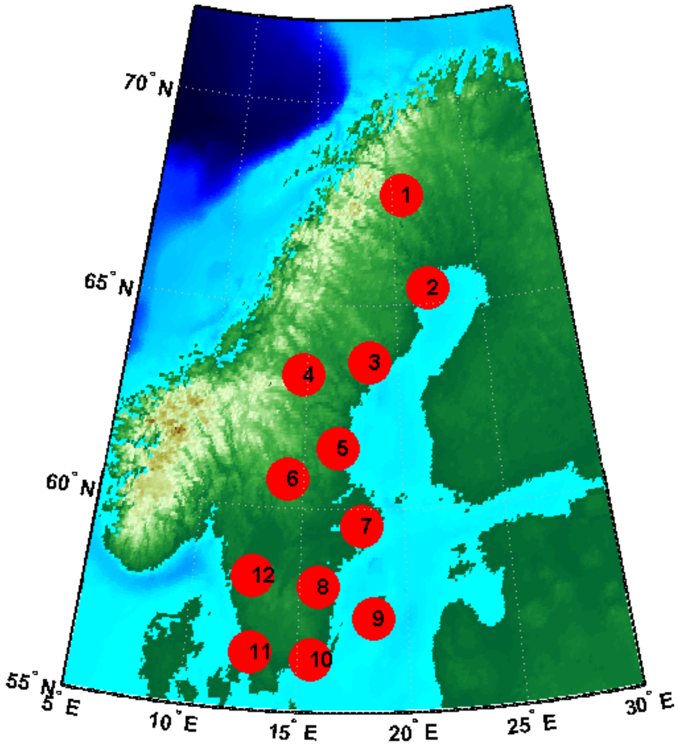

Fig. 1. Geographical position of 12 radars in Sweden.

AMTD
6, 10699–10730, 2013

Precipitation variability over Sweden

A. Devasthale and L. Norin

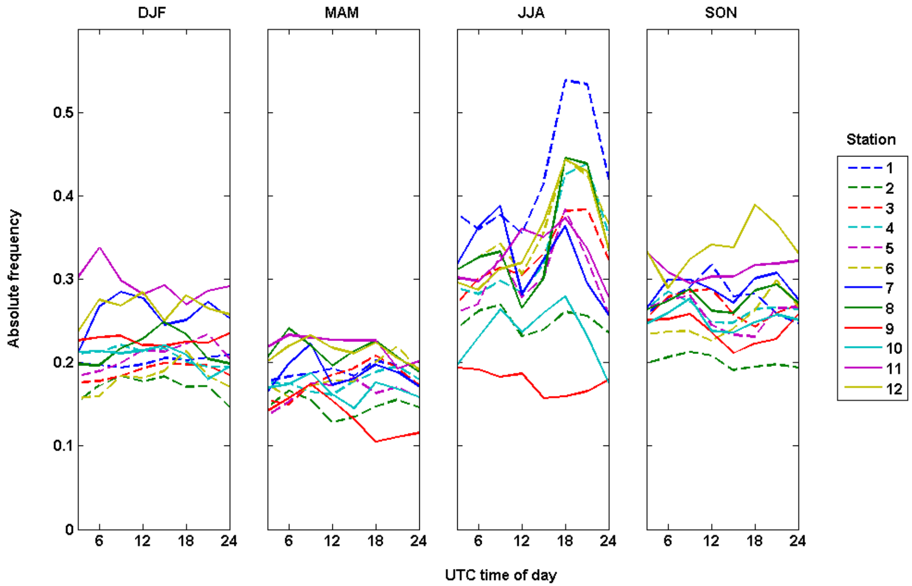

Fig. 2. Diurnal cycle of total precipitation for the 12 radar stations and its seasonal variation. The values on *x* axis are UTC hours.

AMTD
6, 10699–10730, 2013

A. Devasthale and L. Norin

Title Page
Abstract
Introduction
Conclusions
References
Tables
Figures
◀
▶
Back
Close
Full Screen / Esc
Printer-friendly Version
Interactive Discussion

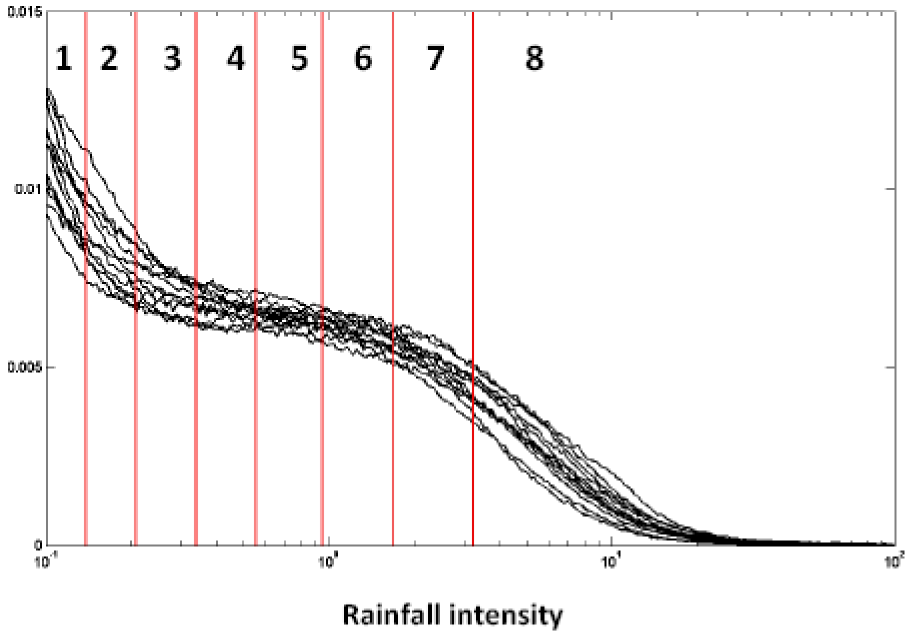

Fig. 3. Normalized frequency of occurrence of accumulated precipitation intensity (mm (3 h)$^{-1}$) for the 12 radar stations based on the entire data record (2000–2010). The vertical lines show 8 bins chosen in such a way that the number of observations is roughly similar in each intensity bin.

AMTD
6, 10699–10730, 2013

CC BY

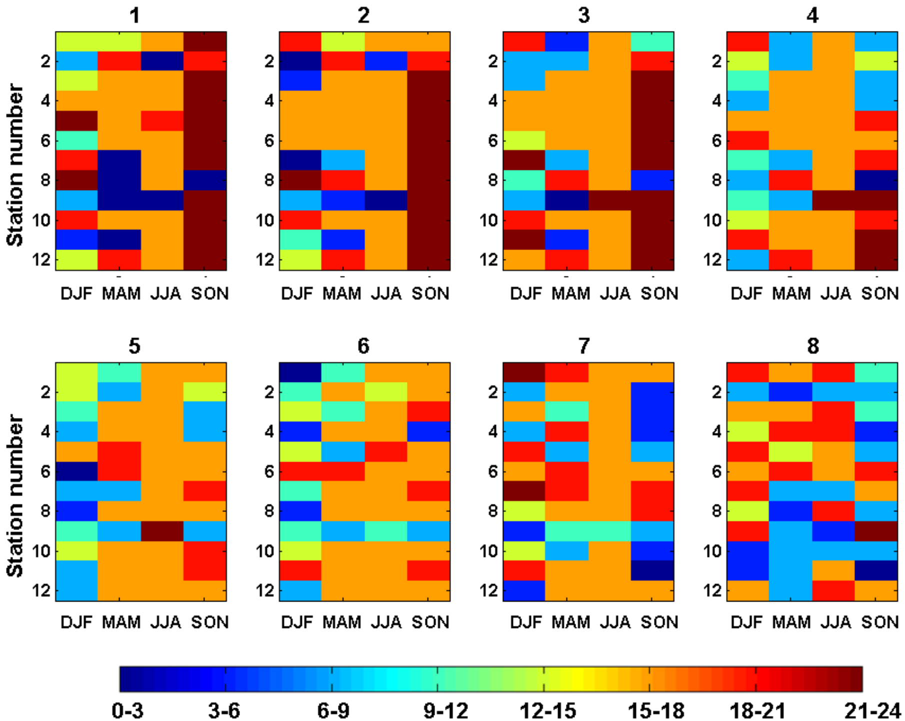

Fig. 4. UTC time (hour of a day) of the diurnal cycle peak. Eight subplots correspond to eight precipitation intensity bins defined in Table 3, and each subplot shows peak times for the 12 stations and 4 seasons.

AMTD
6, 10699–10730, 2013

A. Devasthale and L. Norin

CC BY

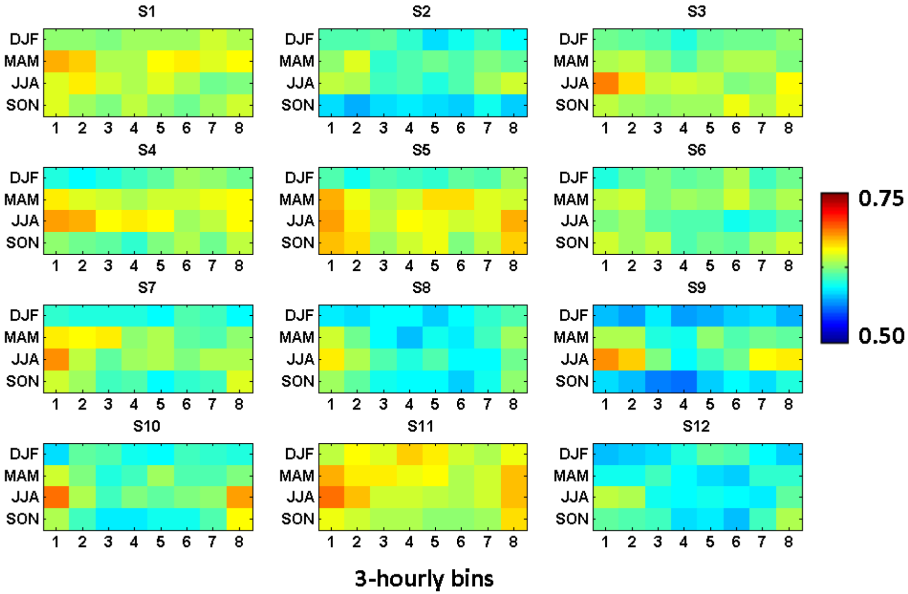

Fig. 5. Coefficient of variation (standard deviation divided by mean) for precipitation for each 3 h bin and season. The 12 subplots correspond to the 12 radar stations (denoted by S1 to S12) over Sweden. The geographical location of these stations is shown in Fig. 1. The 3 h bins numbered from 1 to 8 are UTC hours from 00:00–03:00, 03:00–06:00, 06:00–09:00, 09:00–12:00, 12:00–15:00, 15:00–18:00, 18:00–21:00 and 21:00–24:00 respectively.

AMTD
6, 10699–10730, 2013

Precipitation variability over Sweden

A. Devasthale and L. Norin

CC BY

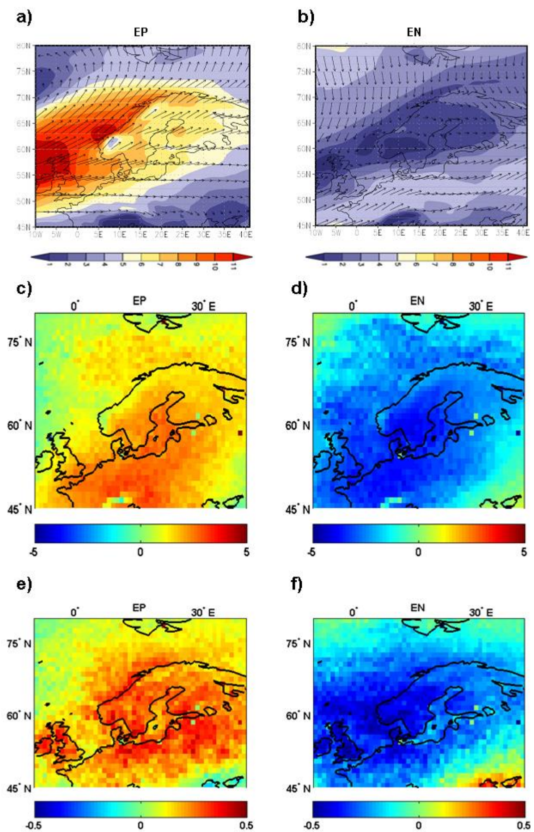

Fig. 6. An overview of meteorological conditions at 850 hPa during enhanced positive (EP) and negative (EN) phases of the Arctic Oscillation. The top row (**a** and **b**) shows wind conditions ($\mathrm{m\,s^{-1}}$), the middle row show temperature anomalies (**c** and **d**; in K) and the bottom row shows water vapour mass mixing ratio anomalies (**e** and **f**; in $\mathrm{g\,kg^{-1}}$).

AMTD
6, 10699–10730, 2013

cc BY

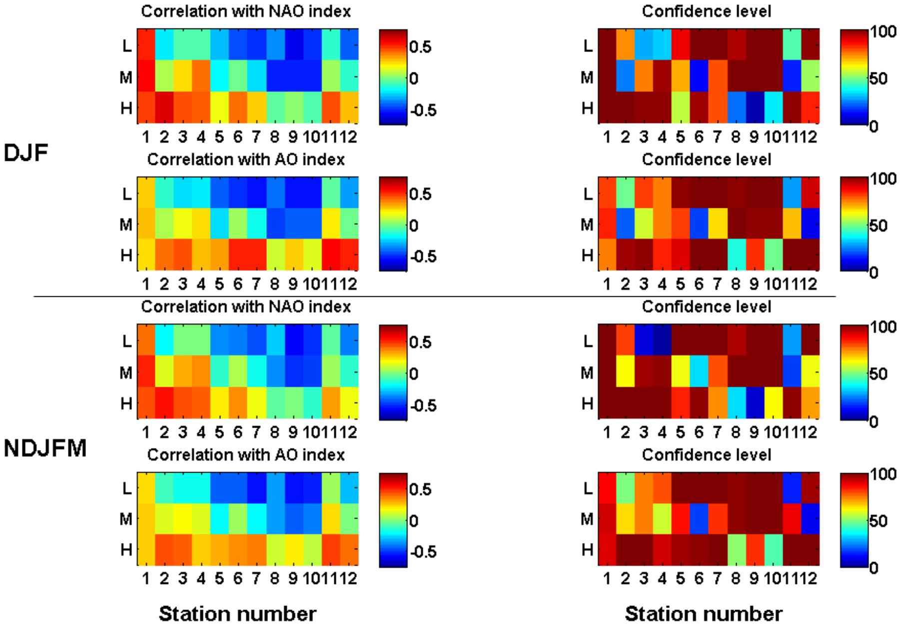

Fig. 7. Correlation of low (L, intensity < 0.34 mm (3 h)$^{-1}$), medium (M, 0.34 < intensity < 1.7 mm (3 h)$^{-1}$) and high (H, intensity > 1.7 mm (3 h)$^{-1}$) intensity precipitation events (left column) with the NAO and AO indices over the 12 radar stations. The top two rows show results for the DJF months, while the bottom two rows for the NDJFM months. The right column shows confidence levels (0–100 %) at which the observed correlations are significant.

CC BY

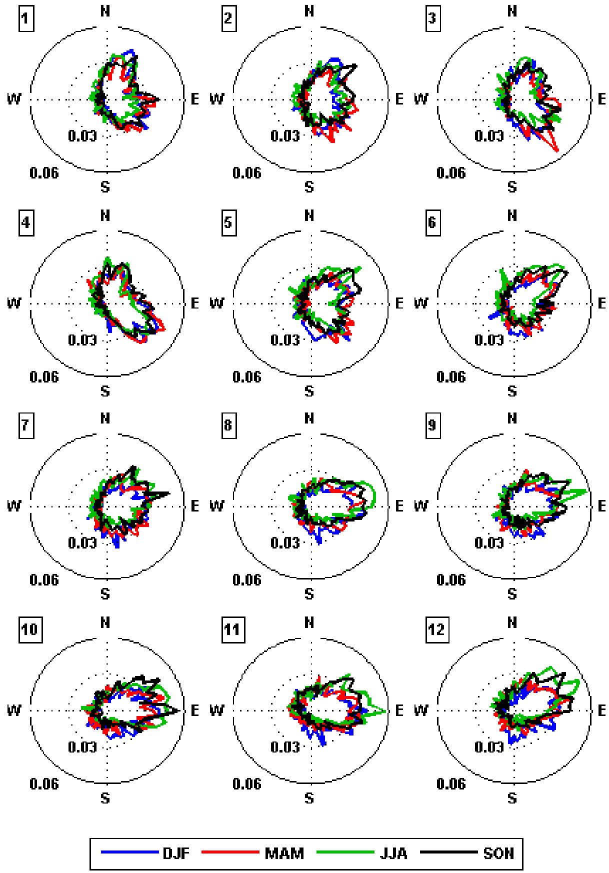

Fig. 8. Distribution of wind direction at 12 radar stations during different seasons based on the data from ERA-Interm reanalysis.

AMTD
6, 10699–10730, 2013

Precipitation variability over Sweden

A. Devasthale and L. Norin

CC BY

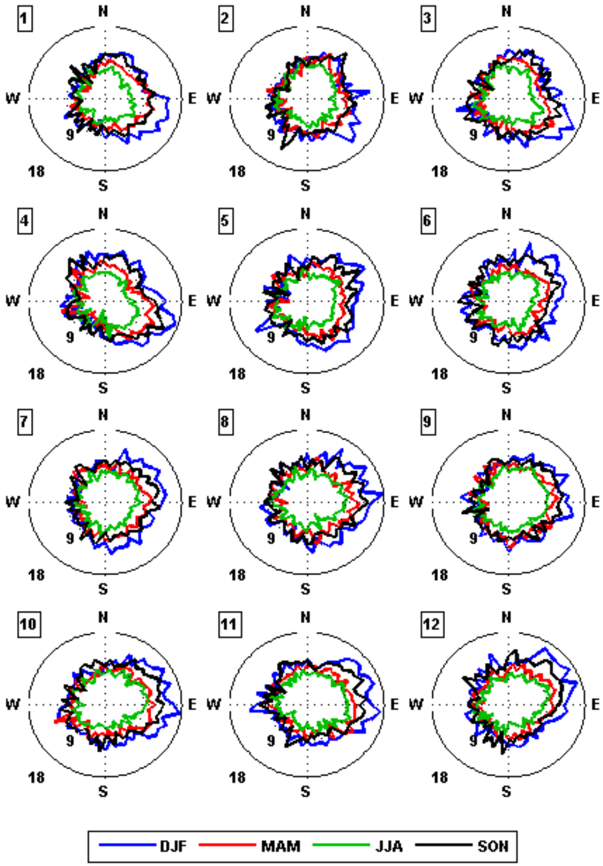

Fig. 9. Average wind speed corresponding to the wind directions shown in Fig. 8 at 12 radar stations during different seasons based on the data from ERA-Interm reanalysis.

AMTD
6, 10699–10730, 2013

Precipitation variability over Sweden

A. Devasthale and L. Norin

Title Page
Abstract Introduction
Conclusions References
Tables Figures
◀| |▶
◀ ▶
Back Close
Full Screen / Esc
Printer-friendly Version
Interactive Discussion

CC BY

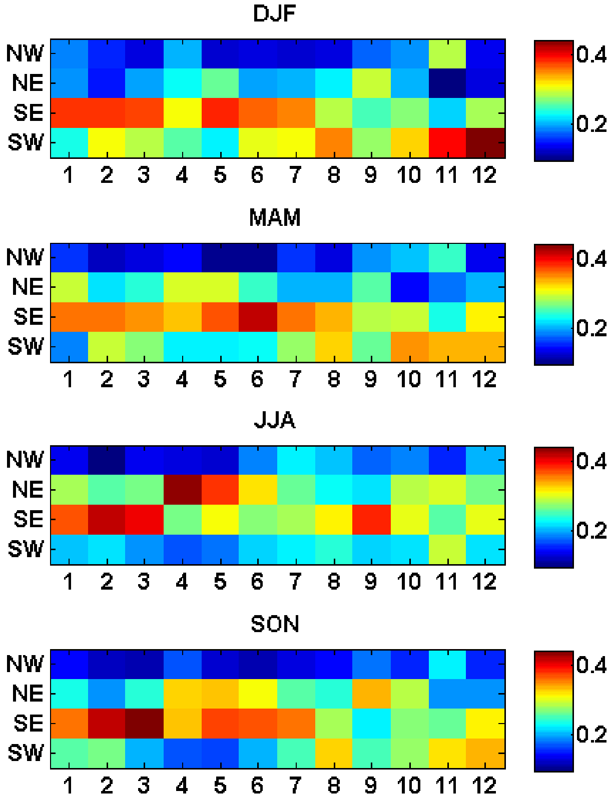

Fig. 10. Relative contribution of wind direction to the average daily rain rate at each of 12 radar stations.

AMTD
6, 10699–10730, 2013

Precipitation variability over Sweden

A. Devasthale and L. Norin

Title Page
Abstract Introduction
Conclusions References
Tables Figures
◀| |▶
◀ ▶
Back Close
Full Screen / Esc
Printer-friendly Version
Interactive Discussion

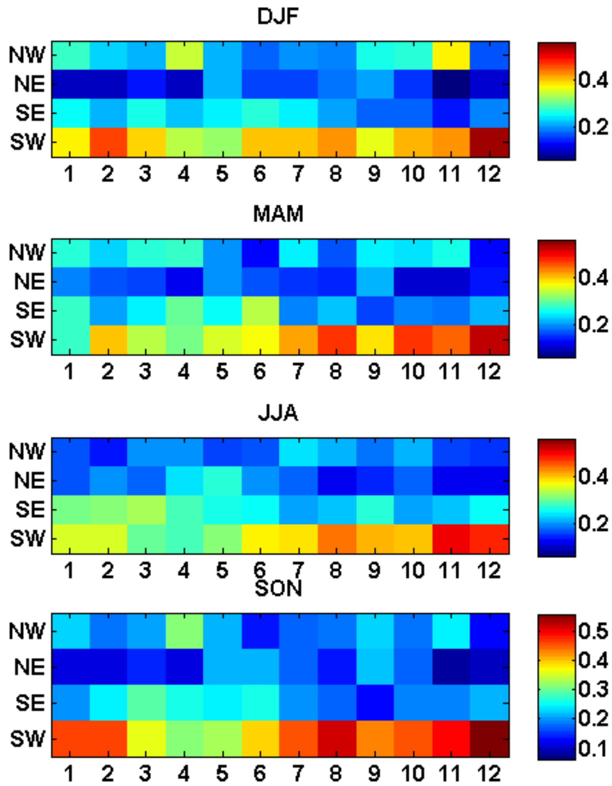

Fig. 11. Same as in Fig. 10, but normalized by the total precipitation occurrences.

AMTD
6, 10699–10730, 2013

Precipitation variability over Sweden

A. Devasthale and L. Norin

CC BY

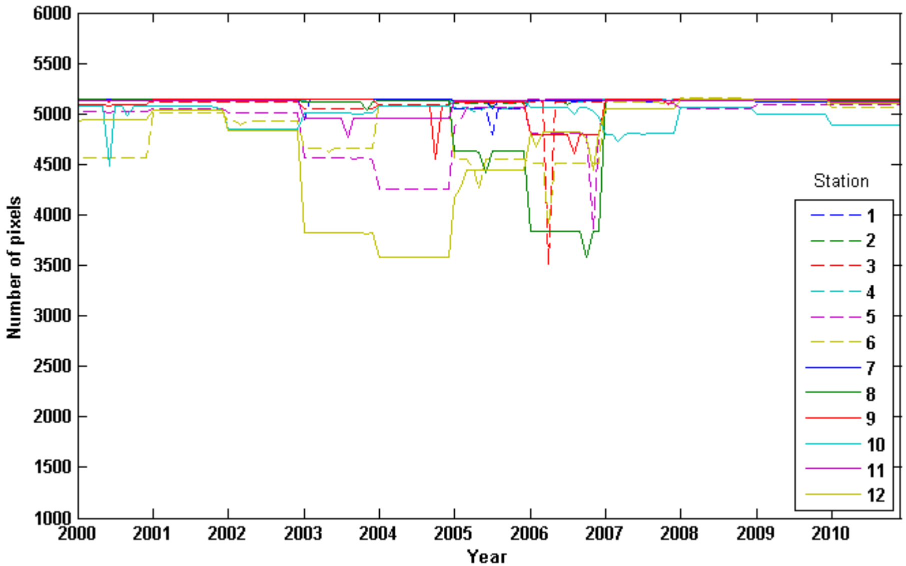

Fig. A1. The number of average monthly pixels from each of the 12 radars used in the analysis.

AMTD
6, 10699–10730, 2013

Precipitation variability over Sweden

A. Devasthale and L. Norin